**Contents**

# I. SIMULATIONS

## A. Event generator for $ep \to ep\pi^+\pi^-$

The previously available version of the two-pion event generator was written in FORTRAN and has several limitations. It employs $\pi^+\pi^- p$ differential cross sections from the older JM05 version of the JM model [1–3]. During the past several years the model was further developed [4] and significantly improved. Furthermore, the two-pion part of that event generator is only applicable up to 2 GeV in $W$ and from 0.3 GeV$^2$ in $Q^2$, and therefore excludes most of the region of interest (high $W$ and low $Q^2$), where it uses simple interpolations. Therefore the substantial need to develop new event generator emerged, and it was successfully developed for this Proposal.

The new event generator employs the 5-fold differential cross sections from the recent version of the JM15 model fit to all results on charged double pion photo- and electroproduction cross sections from CLAS (both the published and preliminary [5–8]). In the areas covered by CLAS data new event generator successfully reproduces the available integrated and single differential $2\pi$ cross sections. The quality of the description is illustrated in Fig. 1 for several $Q^2$ bins in comparison with the available electroporoduction data [5–7].

In order to extend event generator coverage to the area not covered by CLAS data special extrapolation procedure was applied. For that purpose other available world data on $W$ dependencies of $2\pi$ photoproduction integrated cross sections were used [9, 10]. The use of this approach allows to generate $2\pi$ events at extremely low $Q^2$ (less than 0.1 GeV$^2$) and high $W$ (up to 3 GeV). On left side in Fig. 2 the $W$ dependence of integrated cross section for quasi-real $Q^2$ (0.0015 GeV$^2$) is shown in comparison with data [8–10]. The right side of Fig. 2 illustrates a typical example of $Q^2$ dependence of the total cross section for one $W$ bin in comparison with JM15 [4] for beam energy 8.8 GeV.

Besides new event generator has the following advantages. It generates phase space distributions and applies multidimensional cross section as a weight for each event. This method allows us to speed up significantly generation process especially in the areas with sharp cross section dependencies. Also this way of generation makes it possible to obtain absolute values of cross section from generated distributions that is very helpful for various additional purposes such as cross section predictions in areas not covered by experiment.

New event $2\pi$ generator is written on C++, includes inclusive radiative effects according to approach [11] and produces output compatible with the new CLAS12 reconstruction software.

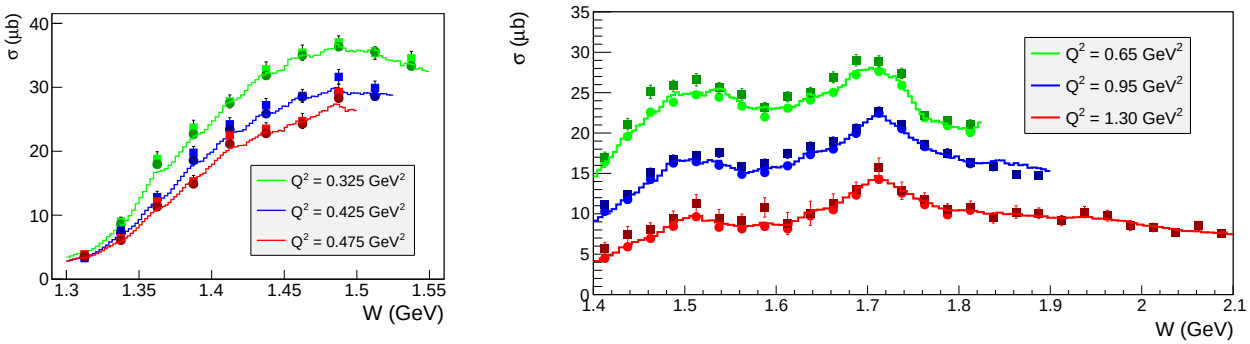


FIG. 1: Comparison between event distributions of the new two-pion event generator (curves) with the integrated cross sections from JM model (circles) and data (squares). Left plot shows the $W$ dependence of the total cross section for three $Q^2$ bins in comparison with the model [6] and data [7] for the corresponding three $Q^2$ points at 0.325, 0.425, and 0.475 GeV$^2$. Right plot shows the $W$ dependence of the total cross section for three $Q^2$ bins in comparison with the model [4] and data [5] for the corresponding three $Q^2$ points at 0.65, 0.95, and 1.3 GeV$^2$.

Studies of run conditions for this Proposal were carried out with new $2\pi$ event generator described above. Exclusive events for $\pi^+\pi^-$ electroproduction off proton were generated in the range of invariant masses of the final hadron system $W$ from the two-pion production threshold to 3 GeV and at photon virtualities $Q^2$ from 0.01 GeV$^2$ to 2.0 GeV$^2$ (see Fig. 3) .

## B. Acceptance estimates for $ep \to ep\pi^+\pi^-$

For the event reconstruction a simplified version of the CLAS12 event reconstruction software, the so-called FASTMC routine, was employed to filter the generated events for acceptance. This routine accounts for the detector fiducial areas and provides smearing over the final particle angles and momenta. The accepted events are

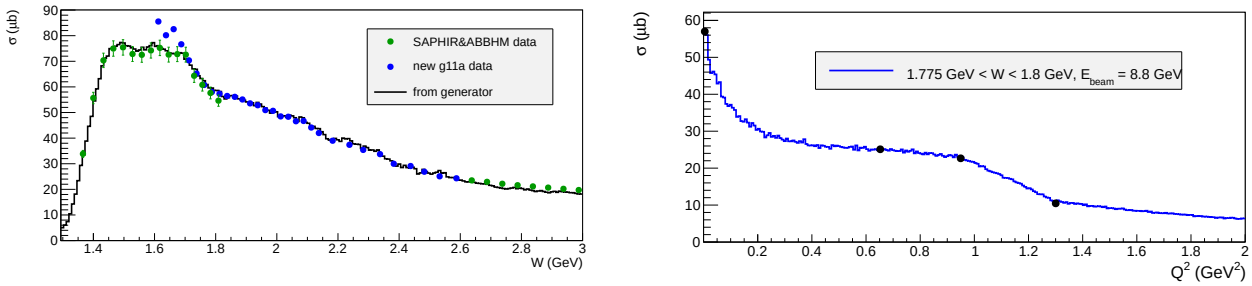


FIG. 2: Left plot shows the $W$ dependence of integrated cross section for quasi-real $Q^2$ (0.0015 GeV$^2$) in comparison with data [8–10]. Right plot shows a typical example of $Q^2$ dependence of the total cross section for one $W$ bin in comparison with JM15 [4] at $W = 1.7875$ GeV for beam energy 8.8 GeV.

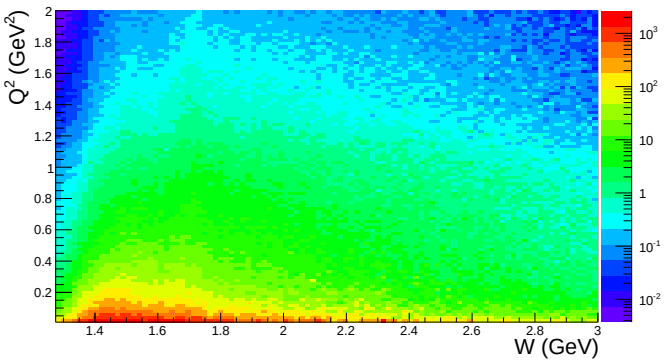


FIG. 3: $Q^2$ versus $W$ distribution for the generated $\pi^+\pi^-p$ events with an electron beam energy of 6.6 GeV. The GENEV event generator based on JM05 [1–3] was used to generate $10^6$ events.

shown in Fig. 4 and are plotted in the $Q^2$ versus $W$ plane. Left and right panels show distributions for reconstructed $\pi^+\pi^-p$ events at two beam energies. The torus current was set to +3375 A, which forces negatively charged particles to bend towards the beam line. The areas of zero acceptance seen in the plots represent the gap between the Forward Tagger and the minimum polar angle accepted in CLAS12 for inbending particles. For the hybrid baryon search the area of small photon virtuality is of particular interest. The size of the gap depends on the torus current setting and the momentum of the scattered electrons. For a negative Torus current, i.e. outbending electrons, the gap is simply given by the geometrical acceptance of CLAS12 and is largely independent of the particle momentum, while for inbending particles the acceptance depends on scattering angle, particle momentum, and magnetic field strength. The acceptance for electron scattering angles from 2.5° to 4.5°, which is covered by the FT, is independent of the torus current settings. In order to cover photon virtualities as low as 0.05 GeV$^2$ measurements with 6.6 GeV electron beam energy are required. The minimal $Q^2$ values for reconstructed events increase up to 0.13 GeV$^2$ for beam energy of 8.8 GeV.

With a beam energy of 6.6 GeV, the influence of the magnetic field direction on the accessible kinematical coverage for $\pi^+\pi^-p$ electroproduction was further studied. The $Q^2$ versus $W$ distributions for reconstructed $\pi^+\pi^-p$ events are shown in Fig. 5 for two opposite polarities of the torus current, +3375 A and -3375 A, which correspond to the maximum expected currents. A wide area of zero acceptance for the normal (+3375 A) direction of the magnetic field is clearly seen in Figure 5 (left). Reversing the magnetic field allows us to decrease substantially the inefficient area, as is shown in Fig. 5 (right). Therefore, the reversed magnetic field represents the best configuration for the proposed experiment, as well as for other experiments, for which the area of small photon virtualities is of particular interest.

We also examined the evolution of counting rates as a function of the magnetic field strength. The 2D $Q^2$ versus $W$ distributions for the accepted $\pi^+\pi^-p$ events are shown in Fig. 6 for the torus currents, -3375 A (left) and -1500 A (right), that correspond to the full and less than half strength magnetic fields for the CLAS12 detector. Comparing the reconstructed event rates shown in Fig. 6, we expect the counting rate to increase by almost a factor of two at half strength of the magnetic field, because of the improved acceptance for the detection of all three $\pi^+\pi^-p$ particles in the final state and the scattered electron. From the other hand decreasing of the torus current will negatively affect particles momentum resolution. So, compromise between this two factors is needed.

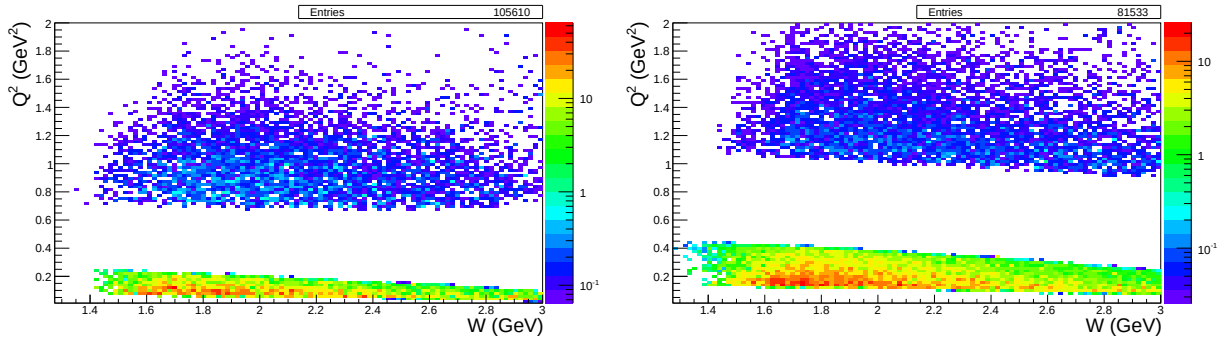


FIG. 4: $Q^2$ versus $W$ distributions for the reconstructed $\pi^+\pi^-p$ events (all particles in final state are registered). Left and right plots correspond to 6.6 GeV and 8.8 GeV beam energies, respectively. The torus current is set to + 3375 A.

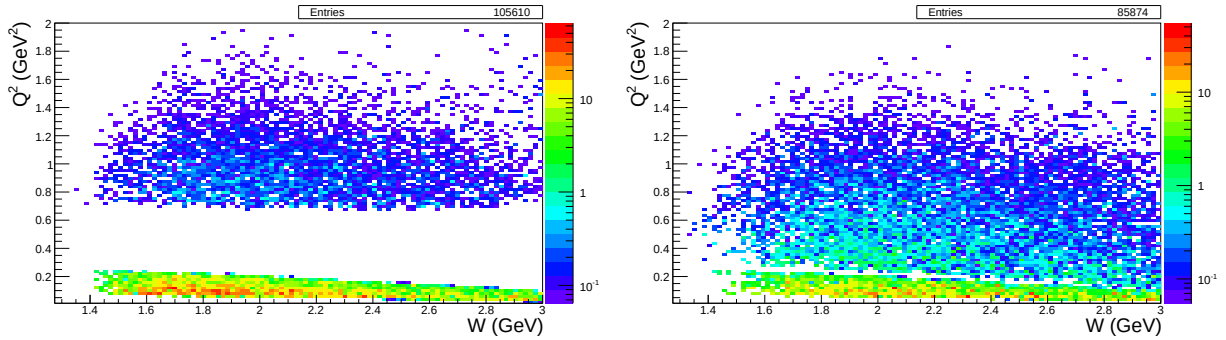


FIG. 5: $Q^2$ versus $W$ distributions for reconstructed $\pi^+\pi^-p$ events (all particles in final state are registered) for the torus currents +3375 A (left) and -3375 A (right). The reversed magnetic field closes the gap between the Forward Tagger and CLAS12.

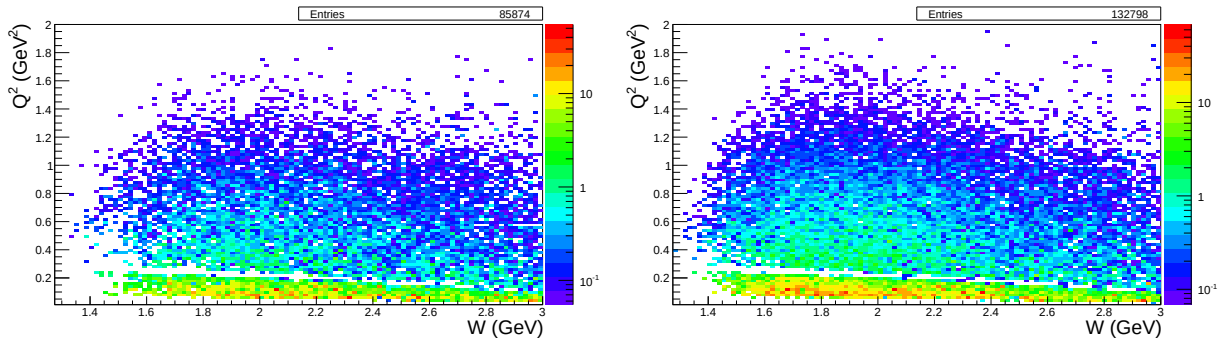


FIG. 6: $Q^2$ versus W distributions for reconstructed $\pi^+\pi^-p$ events at 6.6 GeV beam energy (all final state particles are registered) with torus currents: -3375A (left) and -1500A (right). With lower torus current more events are reconstructed.

### C. Resolution in hadronic mass reconstruction and background estimation for $ep \to ep\pi^+\pi^-$

The hadronic mass resolution is of particular importance in studies of excited nucleon states, since this quantity determines the ability to reliably extract the resonant contributions in exclusive cross sections. For a credible separation between the resonant and the non-resonant contributions the resolution over $W$ should be much smaller than the N* decay width. Typical values for the decay widths of nucleon resonances with masses $> 2.0$ GeV are in a range from 250 to 400 MeV. Hence a mass resolution of $\approx 30$ MeV is sufficient for the reliable isolation of contributions from hybrid-baryons that are expected in the mass range from 2.0 to 3.0 GeV. The resolution in $W$ for the reconstructed $\pi^+\pi^-p$ events was studied in the following way. For each reconstructed event we compute the difference between the exact $W_{gen}$ and the reconstructed $W_{rec}$. We compare two different ways of determining the invariant mass of the final hadron system: a) from the difference between the four-momenta of the initial and the scattered electrons that is added to the four-momentum of the target proton (electron scattering kinematics) b) from the sum of the four-

| Energy (GeV) | Torus current (A) | Eff. all reg. (%) | Eff. $\pi^+$ miss (%) | Eff. $\pi^-$ miss(%) | Eff. proton miss(%) | $Q^2_{min}$ (GeV$^2$) | $\sigma$(W) (GeV) | $\sigma(\sqrt{s})$ (GeV) |
|---|---|---|---|---|---|---|---|---|
| 8.8 | +3375 | 8.2 | 9.8 | 10.3 | 8.6 | 0.13 | 35 | 11 |
| **8.8** | **-3375** | **8.3** | **12.7** | **10.6** | **12.1** | **0.13** | **33** | **10** |
| 8.8 | +1500 | 11.5 | 12.9 | 11.9 | 11.6 | 0.13 | 35 | 11 |
| 8.8 | -1500 | 12.8 | 16.8 | 13.5 | 16.0 | 0.13 | 36 | 11 |
| 6.6 | +3375 | 10.6 | 13.0 | 14.1 | 11.4 | 0.05 | 27 | 11 |
| **6.6** | **-3375** | **8.7** | **13.8** | **11.5** | **13.1** | **0.05** | **26** | **10** |
| 6.6 | +1500 | 15.0 | 17.3 | 16.3 | 15.7 | 0.05 | 25 | 11 |
| 6.6 | -1500 | 13.4 | 18.4 | 14.8 | 17.7 | 0.05 | 29 | 10 |

TABLE I: Comparison of run conditions for the $\pi^+\pi^-p$ channel. Bold rows represent the optimal run conditions for 6.6 and 8.8 GeV beam energy runs.

momenta of the final $\pi^+$, $\pi^-$, and proton (hadron kinematics). The reconstructed $W_{gen}$ - $W_{rec}$ event distributions provide the necessary information on the invariant mass resolution.

The aforementioned distributions for the electron scattering and hadron kinematics are shown in Fig. 7. The beam energy is set to 6.6 GeV and torus current to -1500 A. For both ways of determining the $W_{rec}$ value, the resolution over the full $W$ range is better than 30 MeV and sufficient for the separation of resonant/non-resonant contributions. If $W_{rec}$ is computed from the hadron kinematics, the resolution is significantly better than in the case of electron scattering kinematics. However, the hadron kinematics requires the registration of all final hadrons with a detection efficiency lower than in the inclusive case where the value of $W_{rec}$ is determined from the electron scattering kinematics.

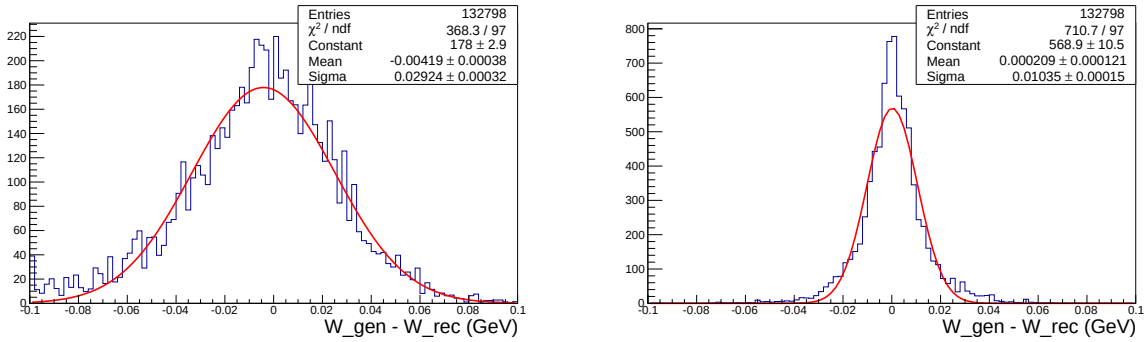


FIG. 7: The $W_{gen} - W_{rec}$ distributions for $\pi^+\pi^-p$ events where $W_{rec}$ is determined by electron scattering (left) and hadron (right) kinematics. See text for explanation of both kinematics.

The studies of charged double pion electroproduction with the CLAS detector [5, 7] demonstrated that the topology, where the final $\pi^-$ is not detected and its four-momentum is reconstructed from energy-momentum conservation, provides the dominant part of the statistics. Hence topologies in which one of the final hadrons is not detected will provide the dominant statistics also in the proposed experiment. We are planning to select the $\pi^+\pi^-p$ events by employing exclusivity cuts on the missing mass squared distributions of any of the final hadrons. The contribution from other exclusive channels (exclusive background) to the events within the exclusivity cuts was evaluated in the Monte-Carlo simulation. Most of the exclusive background events come from the $ep \to e'p'\pi^+\pi^-\pi^0$ channel. Both $\pi^+\pi^-p$ and $3\pi$ events were generated for $W > 2$ GeV. Cross sections of $2\pi$ and $3\pi$ channels were assumed comparable in this kinematic region. A phase space distribution is assumed for the $3\pi$ events. With this mixture of generated events we reconstructed the $\pi^+\pi^-p$ events and determined their distribution over the missing mass squared for $\pi^+$ and $\pi^-$. They are plotted in Fig. 8. The blue curves in Fig. 8 show the $2\pi$ event contributions and the green curves represent the $3\pi$ event contributions. The exclusivity cuts provide good isolation of the $\pi^+\pi^-p$ events with the following contributions from the $3\pi$ events: about 3% for $\pi^+$ missing topology and 4% for $\pi^-$ missing topology.

### D. Summary of experimental condition study

The summary of the run conditions studied in the simulations described above is listed in Table I. Bold rows correspond to the optimal set-up for the proposed experiment.

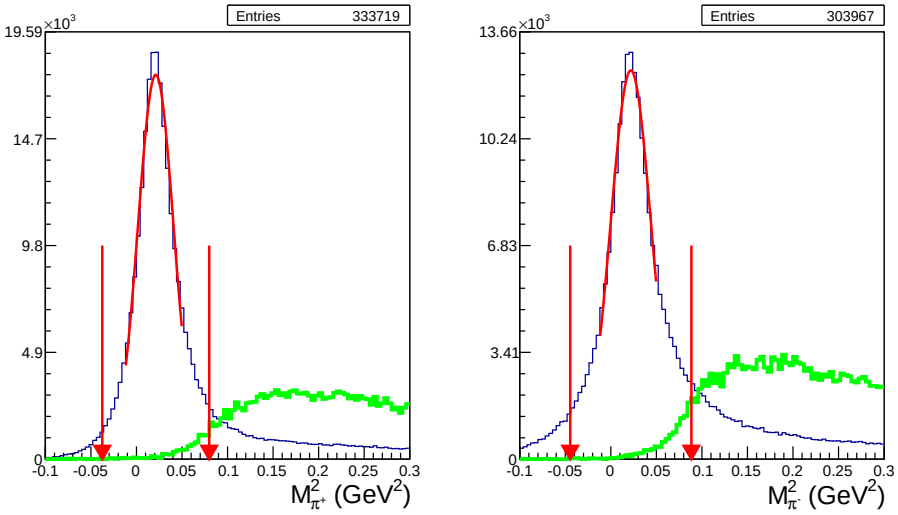


FIG. 8: The reconstructed $\pi^+\pi^-p$ event distributions of the missing masses squared of $\pi^+$ (left) and $\pi^-$ (right) for the generated $\pi^+\pi^-p$ events with an admixture of $3\pi$ events. The distributions were plotted for $W > 2$ GeV. Cross sections of $2\pi$ and $3\pi$ channels were assumed comparable in this kinematic region. The contributions from the $\pi^+\pi^-p$ and the $\pi^+\pi^-\pi^0p$ events are shown in blue and green, respectively. The red arrows indicate the applied exclusivity cuts.

Whereas the summary of the kinematical coverage in terms of 2D plots of $\phi$ versus $\theta$ distributions for the final hadrons is shown in Fig. 9 for all final hadrons detected, a beam energy of 6.6 GeV, and torus current -1500 A. The vertical strips at $\theta = 40°$ in all plots of Fig. 9 correspond to the detector gap between forward and central parts of CLAS12. Since a reversed torus magnetic field was chosen, the low angle area is better populated for negatively charged particles ($\pi^-$).

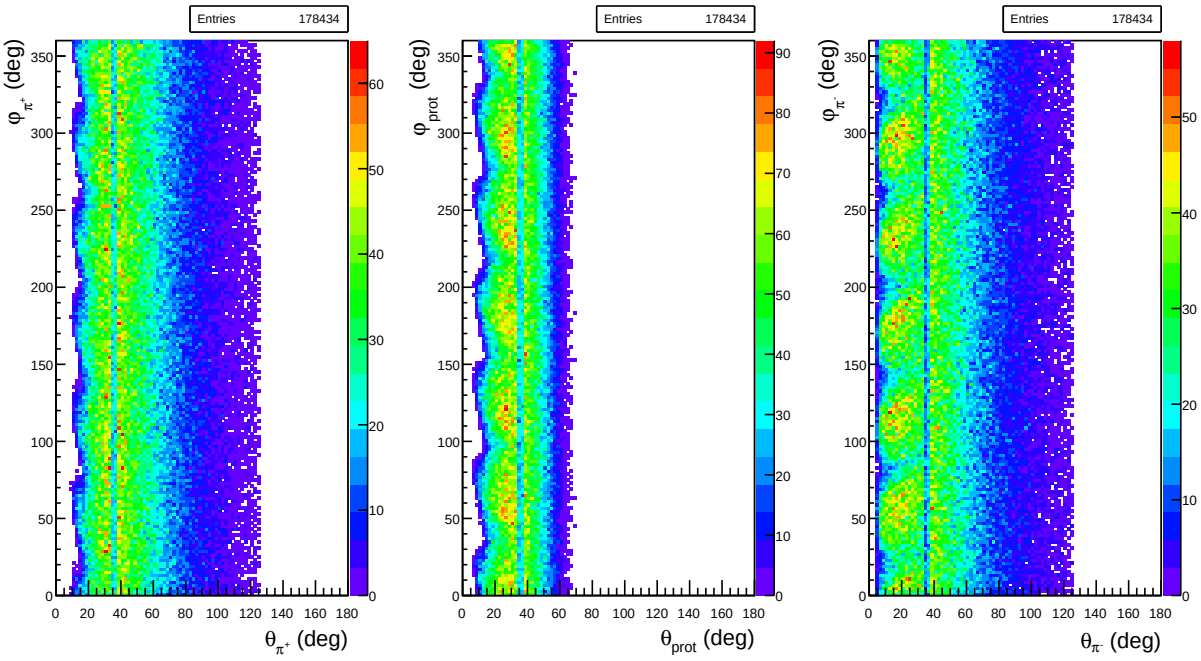


FIG. 9: $\varphi$ vs $\theta$ distributions for the final hadrons: $\pi^+$ (left), proton (middle), and $\pi^-$ (right).

| $Q^2$ (GeV) | 0. | 0.65 | 1.3 |
|---|---|---|---|
| $A_{1/2} \times 10^{-3}$ (GeV$^{-1/2}$) | 45 | 37 | 19 |

TABLE II: Threshold values of $A_{1/2}$ couplings for statistically distinguishable hybrid state signal.

### E. Threshold values of hybrid state couplings

To estimate threshold values of hybrid state couplings that are distinguishable in data analysis phenomenological JM15 [4] model was used. Resonance state with mass 2.2 GeV, width 200 MeV, and J=1/2 was introduced into the model in addition to preliminary established contributions from known resonant states as well as non-resonant mechanisms in the region of $W$ from 2.1 to 2.3 GeV and three $Q^2$ points (quasi real $Q^2 \approx 0$, 0.65, 1.3 GeV$^2$).

The statistical significance of hybrid signal was studied at different values of $A_{1/2}$ electrocoupling using $\chi^2$ criterion. The $\chi^2$ was determined by the following formula (1).

$$\chi^2 = \frac{1}{N_{d.p.}} \sum_{W_i} \sum_{\substack{X=m_{\pi^+\pi^-}, m_{\pi^+p}, \\ \theta_{\pi^-}, \alpha_{\pi^-}}} \left( \frac{\left(\frac{d\sigma_{nohyb}}{dX} - \frac{d\sigma_{hyb}}{dX}\right)^2}{\left(\varepsilon_{nohyb}\frac{d\sigma_{nohyb}}{dX}\right)^2 + \left(\varepsilon_{hyb}\frac{d\sigma_{hyb}}{dX}\right)^2} \right) \tag{1}$$

where $m_{\pi^+\pi^-}$, $m_{\pi^+p}$, $\theta_{\pi^-}$ and $\alpha_{\pi^-}$ are variables that describe final hadron state. $\frac{d\sigma_{nohyb}}{dX}$ - single-fold differential cross section with hybrid $A_{1/2} = 0$. $\frac{d\sigma_{nohyb}}{dX}$ - the same cross section with $A_{1/2}$ equal to certain value. $\varepsilon_{nohyb}$ and $\varepsilon_{hyb}$ - relative statistical uncertainties of single-fold differential cross sections for the cases when hybrid signal is switched off and on respectively. Sums run over all points (from 1 to $N_{d.p.}$) of single-fold differential cross sections for all $W$ bins from 2.1 to 2.3 GeV.

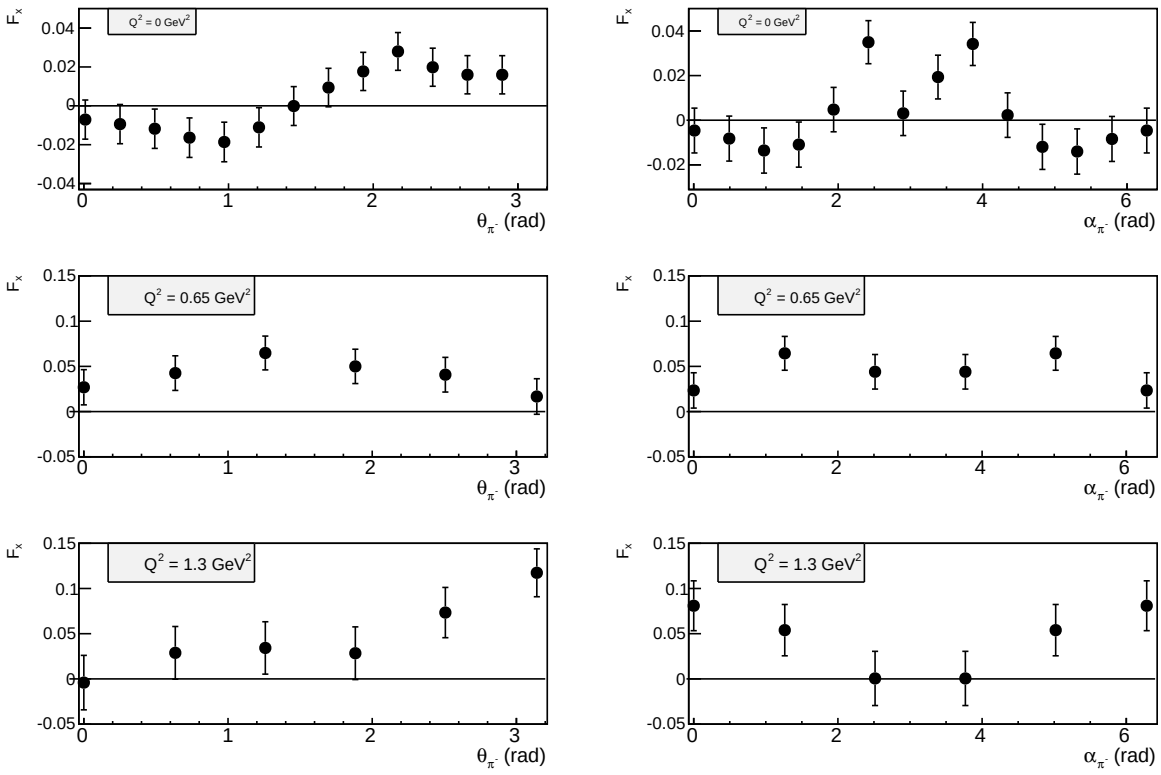


FIG. 10: Relative difference between $2\pi$ cross sections with and without hybrid state as function of angles of final hadrons for three $Q^2$ points.

Statistical uncertainty of single-fold differential cross section with hybrid state was chosen to be the following: 3% at $Q^2 = 1.3$ GeV$^2$,2% at $Q^2 = 0.65$ GeV$^2$, 1% at $Q^2 = 0$ GeV$^2$. This choice was made based on expected reaction

yield roughly estimated in comparison with previous CLAS experiment [5], taking into account that expected DAQ rate in CLAS12 experiments is going to be about ten times higher than in CLAS experiments, run duration is planned to be about two times longer, and $2\pi$ efficiency is expected to be higher up to order of magnitude.

It need to be mentioned that the aforementioned uncertainty estimation is rather conservative in a sense that it implies that just electron trigger will be used. The use of two or three charged particles trigger will lead to the significant increase of $2\pi$ events rate and make statistical uncertainties negligible. Since cross section of $KY$ channel is only few percent from $2\pi$ cross section run condition and trigger choice need to be determined according to $KY$ channel needs.

Statistical uncertainty for single-fold differential cross section without hybrid state ($\varepsilon_{nohyb}$) was assumed to be zero since in model analysis of real data only experimental data points have errors, while the model cross section is fit to the data.

The hybrid signal was considered to be statistically significant if $\chi^2 > 4$. Threshold values of $A_{1/2}$ electrocoupling for statistically significant hybrid state signal are summarized in the Tabl. II. Obtained threshold values of $A_{1/2}$ electrocoupling for hybrid state does not exceed values of electrocouplings for most known resonances in this kinematical region, that makes our estimation very encouraging for the search of new states. If we assume that two or three charged particles trigger is in use the threshold values of electrocouplings are going to be even lower.

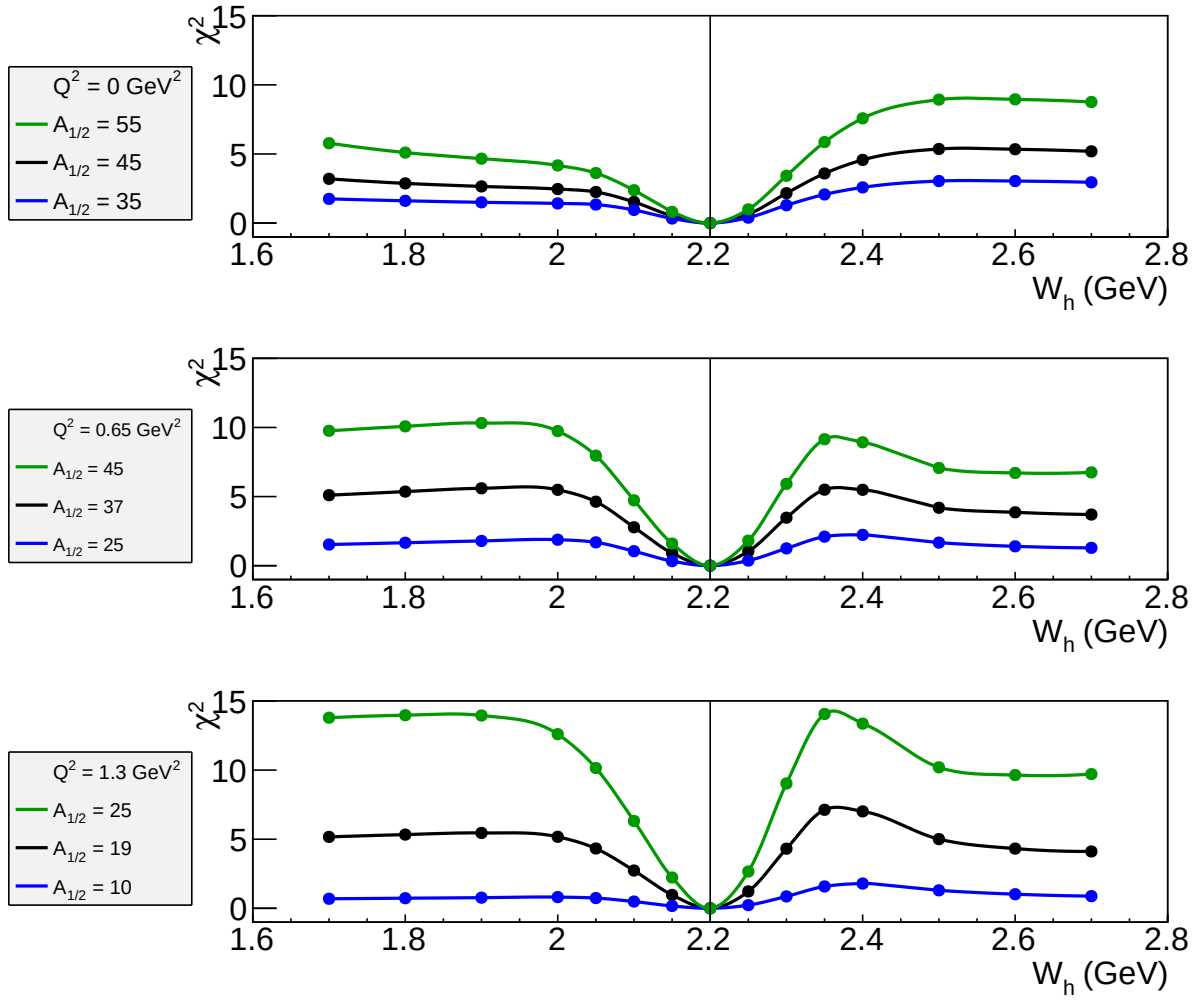


FIG. 11: $\chi^2$ versus $W_h$ distributions for three $Q^2$ values (0 GeV$^2$, 0.65 GeV$^2$, 1.3 GeV$^2$) obtained from JM model. For each value of $Q^2$ the distributions were plotted for three values of $A_{1/2}$ electrocoupling (see legend for each plot).

The hybrid signal manifests mostly in cross section angular distributions. In Fig. 10 the relative difference of $2\pi$ cross section with and without hybrid state are plotted as functions of $\theta_{\pi^-}$ and $\alpha_{\pi^-}$ for three $Q^2$ bins. Distributions in Fig. 10 are produced for th threshold values of $A_{1/2}$ electrocoupling listed in Tabl. II. As it seen from the plots in Fig. 10 this difference grows as $Q^2$ increases, that corresponds to the fact that relative contribution of resonant part to the total $2\pi$ cross section arises with $Q^2$.

The ability of JM model to distinguish hybrid state signal is also illustrated in Fig. 11, where the $\chi^2$ value is plotted as function of resonance mass for three $Q^2$ points and various values of $A_{1/2}$ electrocoupling. The dip in $\chi^2$ dependences is clearly seen on the $W_h$ value corresponded to the expected mass of the hybrid state when $A_{1/2}$ electrocoupling value exceeds threshould.

[1] M. Ripani *et al.*, "A Phenomenological description of $\pi^-\Delta^{++}$ photoproduction and electroproduction in nucleon resonance region," *Nucl. Phys.*, vol. A672, pp. 220–248, 2000.

[2] I. G. Aznauryan, V. D. Burkert, G. V. Fedotov, B. S. Ishkhanov, and V. I. Mokeev, "Electroexcitation of nucleon resonances at $Q^2 = 0.65$ $(\mathrm{GeV/c})^2$ from a combined analysis of single- and double-pion electroproduction data," *Phys. Rev.*, vol. C72, p. 045201, 2005.

[3] V. I. Mokeev, V. D. Burkert, L. Elouadrhiri, A. A. Boluchevsky, G. V. Fedotov, E. L. Isupov, B. S. Ishkhanov, and N. V. Shvedunov, "Phenomenological analysis of the clas data on double charged pion photo and electro-production," in *Proceedings, 5th International Workshop on Physics of excited nucleons (NSTAR 2005)*, pp. 47–56, 2005.

[4] V. I. Mokeev, V. D. Burkert, T.-S. H. Lee, L. Elouadrhiri, G. V. Fedotov, and B. S. Ishkhanov, "Model Analysis of the $p\pi^+\pi^-$ Electroproduction Reaction on the Proton," *Phys. Rev.*, vol. C80, p. 045212, 2009.

[5] M. Ripani *et al.*, "Measurement of $ep \to e'p'\pi^+\pi^-$ and baryon resonance analysis," *Phys. Rev. Lett.*, vol. 91, p. 022002, 2003.

[6] V. I. Mokeev *et al.*, "Experimental Study of the $P_{11}(1440)$ and $D_{13}(1520)$ resonances from CLAS data on $ep \to e'\pi^+\pi^-p'$," *Phys. Rev.*, vol. C86, p. 035203, 2012.

[7] G. V. Fedotov *et al.*, "Electroproduction of $p\pi^+\pi^-$ off protons at $0.2 < Q^2 < 0.6$ GeV$^2$ and $1.3 < W < 1.57$ GeV with CLAS," *Phys. Rev.*, vol. C79, p. 015204, 2009.

[8] E. Golovach *et al.*, "$\gamma p \to p\pi^+\pi^-$ cross sections from g11a experiment," *CLAS ANALYSIS NOTE (under review).*

[9] C. Wu *et al.*, "Photoproduction of $\rho^0$ mesons and Delta-baryons in the reaction $\gamma p \to p\pi^+\pi^-$ at energies up to $s^{1/2} =$ 2.6 GeV," *Eur. Phys. J.*, vol. A23, pp. 317–344, 2005.

[10] "Photoproduction of Meson and Baryon Resonances at Energies up to 5.8 GEV," *Phys. Rev.*, vol. 175, pp. 1669–1696, 1968.

[11] L. W. Mo and Y.-S. Tsai, "Radiative Corrections to Elastic and Inelastic e p and mu p Scattering," *Rev. Mod. Phys.*, vol. 41, pp. 205–235, 1969.